Mon. Not. R. Astron. Soc. **301,** 1064–1072 (1998)

Theory and statistics of weak lensing from large-scale mass inhomogeneities

Marc Kamionkowski,[1,2] Arif Babul,[3,4] Catherine M. Cress[2,5] and Alexandre Refregier[1,2,6]

[1]*Department of Physics, Columbia University, 538 West 120th Street, New York, NY 10027, USA*
[2]*Columbia Astrophysics Laboratory, 538 West 120th Street, New York, NY 10027, USA*
[3]*Department of Physics & Astronomy, University of Victoria, PO Box 3055, Victoria, BC V8W 3P6, Canada*
[4]*Department of Physics, New York University, 4 Washington Place, New York 10003, USA*
[5]*Department of Astronomy, Columbia University, 538 West 120th Street, New York, NY 10027, USA*
[6]*Department of Astrophysical Sciences, Peyton Hall, Princeton University, Princeton, NJ 08544, USA*

Accepted 1998 August 17. Received 1997 December 8

ABSTRACT

Weak lensing by large-scale mass inhomogeneities in the Universe induces correlations in the observed ellipticities of distant sources. We first review the harmonic analysis and statistics required of these correlations and discuss calculations for the predicted signal. We consider the ellipticity correlation function, the mean-square ellipticity, the ellipticity power spectrum and a global maximum-likelihood analysis to isolate a weak-lensing signal from the data. Estimates for the sensitivity of a survey of a given area, surface density, and mean intrinsic source ellipticity are presented. We then apply our results to the FIRST radio-source survey. We predict an rms ellipticity of roughly 0.011 in 1×1 deg^2 pixels and 0.018 in 20×20 arcmin^2 pixels if the power spectrum is normalized to $\sigma_8 \Omega^{0.53} = 0.6$, as indicated by the cluster abundance. The signal is significantly larger in some models if the power spectrum is normalized instead to the *COBE* anisotropy. The uncertainty in the predictions from imprecise knowledge of the FIRST redshift distribution is about 25 per cent in the rms ellipticity. We show that FIRST should be able to make a statistically significant detection of a weak-lensing signal for cluster-abundance-normalized power spectra.

Key words: cosmology: theory – gravitational lensing – large-scale structure of Universe.

1 INTRODUCTION

It has been proposed that the effects of weak lensing on distant sources could shed light on the large-scale distribution of mass in the Universe (Gunn 1967; Miralda-Escudé 1991; Blandford et al. 1991; Kaiser 1992; Bartelmann & Schneider 1992; Kaiser 1998; Villumsen 1996; Stebbins 1996; Jain & Seljak 1997). Mass inhomogeneities along the line of sight to distant sources will induce distortions in the images of these sources; thus, correlations of the ellipticities of distant sources provides a probe of the correlation of mass along the line of sight. In this way, the power spectrum for the *mass* (rather than light) distribution in the Universe can be probed.

This technique requires (i) a sample of sources which are distant, so there is a large line of sight over which the lensing signal can accrue; (ii) good angular resolution, so that the ellipticities of sources can be determined; and (iii) a large enough sample of sources so that the noise provided by the intrinsic ellipticities of sources can be overcome. For example, the VLA FIRST radio survey meets all of these criteria (Becker, White & Helfand 1995; White et al. 1997). Upon completion, the survey will cover 10000 deg^2 of the North Galactic cap. There are $\sim$40 sources per deg^2 with resolved structure on scales from 2−30 arcsec at the survey resolution of 5 arcsec, and the mean redshift of these sources is of order unity. Several systematic effects can produce spurious ellipticity correlations in FIRST, and therefore be mistaken for a weak-lensing signal. However, the most serious systematic effects are understood and can be corrected for (Refregier & Brown 1998; Refregier et al., in preparation).

When looking for the effects of weak lensing on galaxies behind a cluster, one requires tens of thousands of galaxies per arcmin^2 to overcome the Poisson noise from intrinsic galactic ellipticities and thereby map the shear field. With this in mind, it may at first seem hopeless to detect the effects of weak lensing in a sparsely-sampled survey such as FIRST with < 100 resolved sources per deg^2. However, for weak lensing from large-scale structure, we are interested in the correlation of ellipticities of pairs of sources with some fixed angular separation; we do not necessarily need to map the shear field. For this, the relevant quantity is not the density of sources, but the *total* number of pairs of sources in the survey with some fixed angular separation. In other words, the sensitivity to the mean-square ellipticity averaged over regions of some fixed size on the sky is improved with a large area [cf. the discussion of sparse sampling in Kaiser (1998)].

In this paper, we review the theory of ellipticity correlations from

weak gravitational lensing. We discuss statistical techniques which can be used to isolate a signal in the data. We also estimate the amplitude which may be detectable with a survey that covers a given fraction of the sky with a given number of resolved sources per deg^2 and a given mean intrinsic source ellipticity. We then calculate the predicted weak-lensing correlations in the FIRST radio survey for the canonical cold-dark-matter model as well as for several viable variants. We discuss the uncertainties in the predictions that arise from imprecise knowledge of the redshift distribution of FIRST sources, and consider the detectability of the signal. (Refregier & Brown 1998) show how spatial noise correlation, one of the most serious systematic effects for FIRST, affects weak-lensing measurements and can be corrected for. A subsequent paper will present the results of the search for weak lensing in FIRST (Refregier et al. in preparation).

2 ELLIPTICITY CORRELATIONS FROM WEAK LENSING

2.1 Description of the shear field

Weak lensing will induce a stretching of images on the sky at position $\boldsymbol{\theta} = (\theta_x, \theta_y)$ described by the shear field, a symmetric, trace-free 2×2 tensor field:

$$\gamma_{\alpha\beta}(\boldsymbol{\theta}) = \begin{pmatrix} \epsilon_+(\boldsymbol{\theta}) & \epsilon_\times(\boldsymbol{\theta}) \\ \epsilon_\times(\boldsymbol{\theta}) & -\epsilon_+(\boldsymbol{\theta}) \end{pmatrix}. \tag{1}$$

Here, ϵ_+ is the stretching in the $\hat{\theta}_x - \hat{\theta}_y$ directions, and $\epsilon_\times$ is the stretching along axes rotated by 45°. Alternatively, the shear field can be written as a shear 'vector,'

$$\gamma_\alpha = (\epsilon_+, \epsilon_\times) = \gamma(\cos 2\alpha, \sin 2\alpha), \tag{2}$$

although this ordered pair does not transform as a vector. The deformation is also sometimes written as a complex ellipticity p; the two components of the polarization 'vector' are the real and imaginary parts of the complex ellipticity,

$$\begin{aligned} p &= \frac{(a^2 - b^2)}{(a^2 + b^2)} \mathrm{e}^{2\mathrm{i}\alpha} = |p| \mathrm{e}^{2\mathrm{i}\alpha} \\ &= (\epsilon_+^2 + \epsilon_\times^2)^{1/2} \mathrm{e}^{2\mathrm{i}\alpha} = \epsilon_+ + \mathrm{i}\epsilon_\times, \end{aligned} \tag{3}$$

where a and b are the principle moments. We see that $\gamma = |p| = (\epsilon_+^2 + \epsilon_\times^2)^{1/2} = (a^2 - b^2)/(a^2 + b^2)$ and $\tan 2\alpha = \epsilon_\times/\epsilon_+$.

As pointed out by Stebbins (1996), the shear tensor field $\gamma_{\alpha\beta}(\boldsymbol{\theta})$, can be decomposed into a 'gradient' or curl-free component (what Stebbins calls the scalar part) and a 'curl' (or pseudoscalar) component, just as a two-dimensional vector field can be decomposed into curl and curl-free parts. In other words, the shear tensor can be written in terms of two scalar functions $\gamma_\mathrm{g}(\boldsymbol{\theta})$ and $\gamma_\mathrm{c}(\boldsymbol{\theta})$,

$$\nabla^2 \gamma_\mathrm{g} = \partial_\alpha \partial_\beta \gamma_{\alpha\beta}, \quad \nabla^2 \gamma_\mathrm{c} = \epsilon_{\alpha\gamma} \partial_\beta \partial_\gamma \gamma_{\alpha\beta}, \tag{4}$$

where $\epsilon_{\alpha\beta}$ is the antisymmetric tensor. Specification of $\gamma_\mathrm{g}(\boldsymbol{\theta})$ and $\gamma_\mathrm{c}(\boldsymbol{\theta})$ is equivalent to specification of $\epsilon_+(\boldsymbol{\theta})$ and $\epsilon_\times(\boldsymbol{\theta})$. The quantities γ_g and γ_c are the gradient and curl components of the ellipticity field.

Density perturbations (mass inhomogeneities) produce only scalar perturbations to the space–time metric, so they have no handedness and can therefore produce no curl. Gravitational waves have a handedness and may induce a non-zero γ_c. However, the weak-lensing signal from gravitational waves is expected to be extremely small (Stebbins 1996). Vector modes could also produce a curl, but, like tensor modes, they are negligible. Therefore, we expect that $\gamma_\mathrm{c} = 0$, and only γ_g should be non-zero. This allows one to isolate the effect of weak lensing and to check for non-lensing ellipticity correlations.

Throughout, we approximate the region of sky surveyed as a flat surface. At first this might seem inappropriate since the FIRST survey covers a good fraction of the sky. However, weak-lensing ellipticity correlations should be most significant only at smaller angular separations, so the inaccuracies which arise from approximating the sky as a flat surface should be small. Furthermore, we are primarily interested here in establishing the existence of an ellipticity correlation. With future more sensitive data, it will be necessary to account for the curvature of the sky (Stebbins 1996).

Given the shear tensor $\gamma_{\alpha\beta}(\boldsymbol{\theta})$, the functions γ_g and γ_c can be constructed only with a Fourier transform. Writing

$$\begin{aligned} \gamma_{\alpha\beta}(\boldsymbol{\theta}) &= \int \frac{\mathrm{d}^2\boldsymbol{\kappa}}{(2\pi)^2} \tilde{\gamma}_{\alpha\beta}(\boldsymbol{\kappa}) \mathrm{e}^{-\mathrm{i}\boldsymbol{\kappa}\cdot\boldsymbol{\theta}}, \\ \tilde{\gamma}_{\alpha\beta}(\boldsymbol{\kappa}) &= \int \mathrm{d}^2\boldsymbol{\theta}\, \gamma_{\alpha\beta}(\boldsymbol{\theta}) \mathrm{e}^{\mathrm{i}\boldsymbol{\kappa}\cdot\boldsymbol{\theta}}, \end{aligned} \tag{5}$$

where the tilde denotes the Fourier transform (and similarly for the other quantities), we get

$$\tilde{\gamma}_\mathrm{g}(\boldsymbol{\kappa}) = \frac{(\kappa_x^2 - \kappa_y^2)\tilde{\epsilon}_+(\boldsymbol{\kappa}) + 2\kappa_x\kappa_y\tilde{\epsilon}_\times(\boldsymbol{\kappa})}{\kappa_x^2 + \kappa_y^2}, \tag{6}$$

$$\tilde{\gamma}_\mathrm{c}(\boldsymbol{\kappa}) = \frac{2\kappa_x\kappa_y\tilde{\epsilon}_+(\boldsymbol{\kappa}) - (\kappa_x^2 - \kappa_y^2)\tilde{\epsilon}_\times(\boldsymbol{\kappa})}{\kappa_x^2 + \kappa_y^2}. \tag{7}$$

The functions $\gamma_\mathrm{g}(\boldsymbol{\theta})$ and $\gamma_\mathrm{c}(\boldsymbol{\theta})$ can then be recovered through the inverse Fourier transformation. Since $\gamma_{\alpha\beta}$ is a real tensor, $\tilde{\gamma}^*_{\alpha\beta}(\boldsymbol{\kappa}) = \tilde{\gamma}_{\alpha\beta}(-\boldsymbol{\kappa})$, and similarly for $\tilde{\gamma}_\mathrm{g}$ and $\tilde{\gamma}_\mathrm{c}$.

2.2 Power spectra

Statistical homogeneity and isotropy guarantee that the two sets of Fourier coefficients, $\tilde{\gamma}_\mathrm{g}$ and $\tilde{\gamma}_\mathrm{c}$, have expectation values,

$$\begin{aligned} \left\langle \tilde{\gamma}^*_\mathrm{g}(\boldsymbol{\kappa}) \tilde{\gamma}_\mathrm{g}(\boldsymbol{\kappa}') \right\rangle &= (2\pi)^2 \delta(\boldsymbol{\kappa} - \boldsymbol{\kappa}') P_{\mathrm{gg}}(\kappa), \\ \left\langle \tilde{\gamma}^*_\mathrm{c}(\boldsymbol{\kappa}) \tilde{\gamma}_\mathrm{c}(\boldsymbol{\kappa}') \right\rangle &= (2\pi)^2 \delta(\boldsymbol{\kappa} - \boldsymbol{\kappa}') P_{\mathrm{cc}}(\kappa), \\ \left\langle \gamma^*_\mathrm{g}(\boldsymbol{\kappa}) \gamma_\mathrm{c}(\boldsymbol{\kappa}') \right\rangle &= (2\pi)^2 \delta(\boldsymbol{\kappa} - \boldsymbol{\kappa}') P_{\mathrm{gc}}(\kappa). \end{aligned} \tag{8}$$

The power spectrum $P_{\mathrm{gg}}(\kappa)$ is precisely Kaiser's (1992) ellipticity power spectrum $P_\epsilon(\kappa)$. The second power spectrum $P_{\mathrm{cc}}(\kappa)$ will be effectively zero because weak lensing from gravitational waves is extremely small. The third, $P_{\mathrm{gc}}(\kappa)$, must be identically zero since it is parity violating – that is, this power spectrum changes sign under the change of coordinates $\hat{\boldsymbol{x}} \longrightarrow -\hat{\boldsymbol{x}}$. Since these latter two power spectra are zero, they can be used to look for non-lensing artifacts in the data.

The mean-square gradient component of the ellipticity is

$$\left\langle \gamma_\mathrm{g}^2 \right\rangle = \int \frac{\mathrm{d}^2\boldsymbol{\kappa}}{(2\pi)^2} P_{\mathrm{gg}}(\kappa). \tag{9}$$

Since the mean-square curl component of the ellipticity is zero, $\left\langle \gamma_\mathrm{g}^2 \right\rangle$ is also the mean-square total ellipticity.

Realistically, the mean-square ellipticity cannot be measured. The actual measured quantity is the mean-square ellipticity smoothed with some window function. Suppose we estimate the shear field at position θ by averaging over all ellipticities, e.g., in a square $\theta_p \times \theta_p$ pixel centred at θ. In that case, we are probing a smoothed shear field,

$$\epsilon_+^\mathrm{s}(\boldsymbol{\theta}) = \int \mathrm{d}^2\boldsymbol{\alpha}\, W(\boldsymbol{\alpha})\, \epsilon_+(\boldsymbol{\theta} + \boldsymbol{\alpha}), \tag{10}$$

where $W(\boldsymbol{\alpha})$ is the window function (e.g., for square pixels, constant inside the pixel, zero outside and normalized to unity), and similarly for $\epsilon_\times^s$. All prior results for the unsmoothed field are generalized to the smoothed field as long as we replace $\tilde{\epsilon}_+(\boldsymbol{\kappa}) \rightarrow \tilde{\epsilon}_+^s(\boldsymbol{\kappa}) = \tilde{\epsilon}_+(\boldsymbol{\kappa})\widetilde{W}(\boldsymbol{\kappa})$, where $\widetilde{W}(\boldsymbol{\kappa})$ is the Fourier transform of $W(\boldsymbol{\theta})$. The mean-square smoothed ellipticity is then

$$\left\langle (\gamma_g^s)^2 \right\rangle = \int \frac{d^2\boldsymbol{\kappa}}{(2\pi)^2} P_{gg}(\kappa)\, |\widetilde{W}(\boldsymbol{\kappa})|^2. \tag{11}$$

In the following, we also use the shorthand $P_{gg}^s(\kappa) \equiv P_{gg}(\kappa)|\widetilde{W}(\boldsymbol{\kappa})|^2$ for the smoothed power spectrum. Although the mean-square ellipticity gives a simple indication of the magnitude of the weak-lensing signal, one can obtain a much more sensitive probe of a signal by taking advantage of the information provided by the complete power spectra (or equivalently, correlation functions), as discussed further below.

2.3 Correlation functions

There are three independent two-point ellipticity correlation functions that can be constructed in configuration space from the three power spectra. Since the components (ϵ_+ and $\epsilon_\times$) of the shear tensor are defined with respect to some set of axes on the sky and transform under rotations, correlation functions of these quantities will depend on the relative orientation of the two points being correlated as well as the separation. However, correlation functions that are independent of the coordinate system can be constructed (Stebbins 1996) in analogy with those needed for CMB polarization correlations (Kamionkowski, Kosowsky & Stebbins 1997). To do so, we define correlation functions of ellipticities ϵ_+^r and $\epsilon_\times^r$ measured with respect to axes which are parallel and perpendicular to the line connecting the two points being correlated. To be explicit, suppose the first point is $\boldsymbol{\theta}_1 = (\theta_{1x}, \theta_{1y})$ and the second is $\boldsymbol{\theta}_2 = (\theta_{2x}, \theta_{2y})$. Then we must rotate the axes by an angle $\phi = \arctan[(\theta_{2y} - \theta_{1y})/(\theta_{2x} - \theta_{1x})]$ to align the rotated x axis with the line connecting the two points. Under this rotation, we get

$$\epsilon_+^r = \epsilon_+ \cos 2\phi + \epsilon_\times \sin 2\phi, \tag{12}$$

$$\epsilon_\times^r = -\epsilon_+ \sin 2\phi + \epsilon_\times \cos 2\phi, \tag{13}$$

at both points. The 2ϕ enters since the ellipticity is unchanged under a rotation by 90°. We can then construct three correlation functions, $\langle \epsilon_+^r \epsilon_+^r \rangle$, $\langle \epsilon_\times^r \epsilon_\times^r \rangle$, $\langle \epsilon_+^r \epsilon_\times^r \rangle$, from the rotated components. Although ϵ_+^r is invariant under reflection along the line connecting the two points being correlated, $\epsilon_\times^r$ changes sign. Therefore, parity invariance demands that $\langle \epsilon_+^r \epsilon_\times^r \rangle = 0$. Statistically significant deviations from zero can be due only to systematic errors in the data.

By setting $\phi = 0$ in Kaiser's equation (2.3.1), we identify $\langle \epsilon_+^r(\boldsymbol{\theta}_0) \epsilon_+^r(\boldsymbol{\theta}_0 + \boldsymbol{\theta}) \rangle = C_1(\theta)$ and $\langle \epsilon_\times^r(\boldsymbol{\theta}_0) \epsilon_\times^r(\boldsymbol{\theta}_0 + \boldsymbol{\theta}) \rangle = C_2(\theta)$. We also verify that $\langle \epsilon_+^r(\boldsymbol{\theta}_0) \epsilon_\times^r(\boldsymbol{\theta}_0 + \boldsymbol{\theta}) \rangle = 0$. In analogy with correlation functions of Stokes parameters of the cosmic microwave background (Kamionkowski et al. 1997), we can write the correlation functions (for any ϕ) in terms of the power spectra as

$$C_1(\theta) + C_2(\theta) = \int_0^\infty \frac{\kappa\, d\kappa}{2\pi} [P_{gg}(\kappa) + P_{cc}(\kappa)] J_0(\kappa\theta) \tag{14}$$

$$C_1(\theta) - C_2(\theta) = \int_0^\infty \frac{\kappa\, d\kappa}{2\pi} [P_{gg}(\kappa) - P_{cc}(\kappa)] J_4(\kappa\theta). \tag{15}$$

In terms of correlation functions of rotated and unrotated ellipticities, and in terms of the complex ellipticity p,

$$\begin{aligned} C_1(\theta) + C_2(\theta) &= \left\langle \epsilon_+^r(\boldsymbol{\theta}_0) \epsilon_+^r(\boldsymbol{\theta}_0 + \boldsymbol{\theta}) \right\rangle + \left\langle \epsilon_\times^r(\boldsymbol{\theta}_0) \epsilon_\times^r(\boldsymbol{\theta}_0 + \boldsymbol{\theta}) \right\rangle \\ &= \left\langle \epsilon_+(\boldsymbol{\theta}_0) \epsilon_+(\boldsymbol{\theta}_0 + \boldsymbol{\theta}) \right\rangle + \left\langle \epsilon_\times(\boldsymbol{\theta}_0) \epsilon_\times(\boldsymbol{\theta}_0 + \boldsymbol{\theta}) \right\rangle \\ &= \mathrm{Re}[p^*(\boldsymbol{\theta}_0) p(\boldsymbol{\theta}_0 + \boldsymbol{\theta})], \end{aligned} \tag{16}$$

$$\begin{aligned} C_1(\theta) - C_2(\theta) &= \langle \epsilon_+^r(\boldsymbol{\theta}_0) \epsilon_+^r(\boldsymbol{\theta}_0 + \boldsymbol{\theta}) \rangle - \langle \epsilon_\times^r(\boldsymbol{\theta}_0) \epsilon_\times^r(\boldsymbol{\theta}_0 + \boldsymbol{\theta}) \rangle \\ &= \cos 4\phi [\langle \epsilon_+(\boldsymbol{\theta}_0) \epsilon_+(\boldsymbol{\theta}_0 + \boldsymbol{\theta}) \rangle \\ &\quad - \langle \epsilon_\times(\boldsymbol{\theta}_0) \epsilon_\times(\boldsymbol{\theta}_0 + \boldsymbol{\theta}) \rangle] \\ &\quad + \sin 4\phi [\langle \epsilon_\times(\boldsymbol{\theta}_0) \epsilon_+(\boldsymbol{\theta}_0 + \boldsymbol{\theta}) \rangle \\ &\quad + \langle \epsilon_+(\boldsymbol{\theta}_0) \epsilon_\times(\boldsymbol{\theta}_0 + \boldsymbol{\theta}) \rangle] \\ &= \mathrm{Re}[p(\boldsymbol{\theta}_0) p(\boldsymbol{\theta}_0 + \boldsymbol{\theta})] \cos 4\phi \\ &\quad + \mathrm{Im}[p(\boldsymbol{\theta}_0) p(\boldsymbol{\theta}_0 + \boldsymbol{\theta})] \sin 4\phi, \end{aligned} \tag{17}$$

where $\boldsymbol{\theta} = \{\theta \cos\phi, \theta \sin\phi\}$. There is also the third linearly independent correlation function,

$$\begin{aligned} C_{\mathrm{cross}}(\theta) &= \left\langle \epsilon_+^r(\boldsymbol{\theta}_0) \epsilon_\times^r(\boldsymbol{\theta}_0 + \boldsymbol{\theta}) \right\rangle + \left\langle \epsilon_\times^r(\boldsymbol{\theta}_0) \epsilon_+^r(\boldsymbol{\theta}_0 + \boldsymbol{\theta}) \right\rangle \\ &= -\sin 4\phi \left[\left\langle \epsilon_+(\boldsymbol{\theta}_0) \epsilon_+(\boldsymbol{\theta}_0 + \boldsymbol{\theta}) \right\rangle - \left\langle \epsilon_\times(\boldsymbol{\theta}_0) \epsilon_\times(\boldsymbol{\theta}_0 + \boldsymbol{\theta}) \right\rangle \right] \\ &\quad + \cos 4\phi \left[\left\langle \epsilon_\times(\boldsymbol{\theta}_0) \epsilon_+(\boldsymbol{\theta}_0 + \boldsymbol{\theta}) \right\rangle + \left\langle \epsilon_+(\boldsymbol{\theta}_0) \epsilon_\times(\boldsymbol{\theta}_0 + \boldsymbol{\theta}) \right\rangle \right] \\ &= -\mathrm{Re}[p(\boldsymbol{\theta}_0) p(\boldsymbol{\theta}_0 + \boldsymbol{\theta})] \sin 4\phi \\ &\quad + \mathrm{Im}[p(\boldsymbol{\theta}_0) p(\boldsymbol{\theta}_0 + \boldsymbol{\theta})] \cos 4\phi, \end{aligned} \tag{18}$$

and parity conservation demands $C_{\mathrm{cross}}(\theta) = 0$. Note that when written in terms of the *un*rotated ellipticities or the complex ellipticity, the sum $C_1(\theta) + C_2(\theta)$ is *in*dependent of ϕ. However, when written in terms of the unrotated ellipticities or complex ellipticity, the difference $C_1(\theta) - C_2(\theta)$ and $C_{\mathrm{cross}}(\theta)$ *does* depend explicitly on ϕ, the relative orientation of the two points being correlated.

The power spectra can be written in terms of the correlation functions as

$$\begin{aligned} P_{gg}(\kappa) &= \frac{\pi}{2} \int \theta d\theta \Big\{ [C_1(\theta) + C_2(\theta)] J_0(\kappa\theta) \\ &\quad + [C_1(\theta) - C_2(\theta)] J_4(\kappa\theta) \Big\} \\ P_{cc}(\kappa) &= \frac{\pi}{2} \int \theta d\theta \Big\{ [C_1(\theta) + C_2(\theta)] J_0(\kappa\theta) \\ &\quad - [C_1(\theta) - C_2(\theta)] J_4(\kappa\theta) \Big\}. \end{aligned} \tag{19}$$

Again, if the second of these is non-zero, it can only be because of non-lensing effects, so construction of this correlation function provides a powerful probe for the presence of non-lensing artifacts in the data.

Of course, correlation functions $C^s(\theta)$ for the smoothed ellipticities can be obtained by replacing ellipticities and power spectra by the smoothed ellipticities and power spectra in all the equations above.

3 STATISTICAL ESTIMATORS

The effects of weak lensing can be uncovered through the measured correlation functions, power spectra, mean-square ellipticities averaged over some given pixel size, or a full maximum-likelihood fit to the data.

The Fourier modes of the shear field owing to weak lensing are statistically independent. Furthermore, if the noise map is orientation independent, then the Fourier modes of the noise will also be statistically independent. Even if we use only the simplest (although not necessarily optimal) estimator for the power spectrum, the mean-square ellipticity, it is better to work in Fourier space. The predicted weak-lensing mean-square ellipticity is due entirely to the gradient component, but randomly oriented intrinsic source

ellipticities should contribute to the mean-square ellipticity equally through the gradient and curl component. The signal-to-noise ratio will therefore be improved with a Fourier transform which allows us to isolate the gradient and curl components.

3.1 Discrete Fourier transforms and statistical noise

We restrict ourselves to a survey which covers a rectangular region of the sky. The analysis can be extended to irregularly-shaped regions of the sky, but only with significant complications. [Simple estimates of the effects of an irregularly-shaped survey that are used for the power spectrum of angular clustering (Baugh & Efsthathiou 1993) are not easily generalized to weak-lensing power spectra.] We first construct pixels of size $\theta_p \times \theta_p$ on the sky. This leaves us with $N_{\rm pix} = N_x \times N_y$ pixels, where $N_x = \theta_x/\theta_p$ and $N_y = \theta_y/\theta_p$ and θ_x and θ_y are the dimensions of the map. The pixels labeled by (i,j) are centred at $\boldsymbol{\theta}_{ij} = (i,j)\theta_p$, and $i = 0, 1, ..., N_x - 1$ and $j = 0, 1, ..., N_y - 1$.

The ellipticities, $\epsilon^{\rm obs}_{+,ij}$ and $\epsilon^{\rm obs}_{\times,ij}$, measured in pixel (i,j) are the sum of a weak-lensing signal and noise that arises from intrinsic source ellipticities and measurement error,

$$\epsilon^{\rm obs}_{+,ij} = \epsilon^{\rm s}_{+,ij} + \epsilon^{\rm n}_{+,ij}, \qquad \epsilon^{\rm obs}_{\times,ij} = \epsilon^{\rm s}_{\times,ij} + \epsilon^{\rm n}_{\times,ij}. \tag{20}$$

We can then use a fast Fourier transform to determine the $N_{\rm pix}$ Fourier coefficients of the survey,

$$\tilde{\epsilon}^{\rm obs}_{+}(\boldsymbol{\kappa}) = \sum_{ij} \epsilon^{\rm obs}_{+,ij} e^{i\boldsymbol{\kappa}\cdot\boldsymbol{\theta}_{ij}}, \quad \tilde{\epsilon}^{\rm obs}_{\times}(\boldsymbol{\kappa}) = \sum_{ij} \epsilon^{\rm obs}_{\times,ij} e^{i\boldsymbol{\kappa}\cdot\boldsymbol{\theta}_{ij}}, \tag{21}$$

for $\boldsymbol{\kappa} = (2\pi/\theta_p)(n/N_x, m/N_y)$, and $n = 0, 1, ..., N_x - 1$ and $m = 0, 1, ..., N_y - 1$.

If the noise terms are all statistically independent with variances σ^2_ϵ [i.e., they satisfy $\langle \epsilon^{\rm n}_{+,ij}\epsilon^{\rm n}_{+,kl}\rangle = \sigma^2_\epsilon \delta_{ik}\delta_{jl}$, $\langle \epsilon^{\rm n}_{\times,ij}\epsilon^{\rm n}_{\times,kl}\rangle = \sigma^2_\epsilon \delta_{ik}\delta_{jl}$, and $\langle \epsilon^{\rm n}_{+,ij}\epsilon^{\rm n}_{\times,kl}\rangle = 0$], then estimators for the mean-square ellipticities are given by

$$\widehat{(\gamma^{\rm s}_{\rm g})^2} = \left[\frac{1}{N^2_{\rm pix}} \sum_{\boldsymbol{\kappa}} |\gamma^{\rm obs}_{\rm g}(\boldsymbol{\kappa})|^2\right] - \sigma^2_\epsilon, \tag{22}$$

$$\widehat{(\gamma^{\rm s}_{\rm c})^2} = \left[\frac{1}{N^2_{\rm pix}} \sum_{\boldsymbol{\kappa}} |\gamma^{\rm obs}_{\rm c}(\boldsymbol{\kappa})|^2\right] - \sigma^2_\epsilon, \tag{23}$$

$$\widehat{(\gamma^{\rm s}_{\rm g})^*\gamma^{\rm s}_{\rm c}} = \left[\frac{1}{N^2_{\rm pix}} \sum_{\boldsymbol{\kappa}} [\gamma^{\rm obs}_{\rm g}(\boldsymbol{\kappa})]^* \gamma^{\rm obs}_{\rm c}(\boldsymbol{\kappa})\right] - P^{\rm n}_{\rm gc}(\kappa). \tag{24}$$

These are estimators for variances of a distribution measured with a finite number of pixels. Therefore, there will be some cosmic variance as well as some pixel-noise variance with which these estimators will recover their expectation values. These variances are

$$\left\langle \left[\widehat{(\gamma^{\rm s}_{\rm g})^2} - (\gamma^{\rm s}_{\rm g})^2\right]^2 \right\rangle = \frac{2}{N_{\rm pix}} \left[\left\langle (\gamma^{\rm s}_{\rm g})^2 \right\rangle + \sigma^2_\epsilon\right]^2, \tag{25}$$

$$\left\langle \left[\widehat{(\gamma^{\rm s}_{\rm c})^2} - (\gamma^{\rm s}_{\rm c})^2\right]^2 \right\rangle = \frac{2}{N_{\rm pix}} \left[\left\langle (\gamma^{\rm s}_{\rm c})^2 \right\rangle + \sigma^2_\epsilon\right]^2, \tag{26}$$

$$\left\langle \left[\widehat{(\gamma^{\rm s}_{\rm g})^*\gamma^{c}_{\rm g}} - (\gamma^{\rm s}_{\rm g})^*\gamma^{\rm s}_{\rm c}\right]^2 \right\rangle = \frac{1}{N_{\rm pix}} \left[\left\langle (\gamma^{\rm s}_{\rm g})^2 \right\rangle + \sigma^2_\epsilon\right] \times \left[\left\langle (\gamma^{\rm s}_{\rm c})^2 \right\rangle + \sigma^2_\epsilon\right]. \tag{27}$$

These results may be obtained in analogy with the derivation for cosmic and pixel-noise variances for a temperature-polarization map of the cosmic microwave background (Knox 1995).

Inserting the null hypothesis of no signal, $\left\langle (\gamma^{\rm s}_{\rm g})^2 \right\rangle = 0$, into equation (25) gives us the statistical limit to the weak-lensing amplitude of this quantity to which we are sensitive. Explicitly, we can be assured a 3σ detection of $(\gamma^{\rm s}_{\rm g})^2$ only if it exceeds $3\sigma^2_\epsilon\sqrt{2/N_{\rm pix}}$.

If the density of resolved sources on the sky is $\bar{n}$ (in units of deg^{-2}) and the mean intrinsic ellipticity of the sources is $\bar{\epsilon}$ (the mean intrinsic value of $|p|$), then $\sigma^2_\epsilon = \bar{\epsilon}^2/(\bar{n}\theta^2_p)$. Therefore, if the area of the survey is A, then the survey will be sensitive (at 1σ) to a mean-square ellipticity,

$$\sigma_{\left\langle (\gamma^{\rm s}_{\rm g})^2\right\rangle} = (0.0075)^2\,(A/10000\,{\rm deg}^2)^{-1/2} \times (\bar{\epsilon}/0.4)^2(\bar{n}/40\,{\rm deg}^{-2})^{-1}(\theta_p/{\rm deg})^{-1}, \tag{28}$$

for pixels of area θ^2_p. Since the signal is the mean-square ellipticity (rather than the rms ellipticity), an rms ellipticity $\gtrsim\sqrt{3}(0.0075) \simeq 0.013$ in 1 deg^2 pixels should be detectable at 3σ with the survey parameters assumed here. The central values above were chosen to be close to those expected for resolved sources in the completed FIRST survey.

3.2 Likelihood analysis

Although the mean-square ellipticity per pixel provides a simple estimate of the sensitivity of a given survey to a signal, it is not the optimal statistic for detecting a weak-lensing signal. The sensitivity of a survey to a weak-lensing signal can be improved significantly with a maximum-likelihood analysis which compares the complete power spectrum (rather than just the mean-square ellipticity) with the entire survey.

Suppose that in a survey with $N_{\rm pix}$ pixels we construct a $2N_{\rm pix}$-dimensional data vector, $D^{\rm obs}_\alpha = \{\epsilon^{\rm obs}_{+,1}, \epsilon^{\rm obs}_{\times,1}, \epsilon^{\rm obs}_{+,2}, \epsilon^{\rm obs}_{\times,2}, ..., \epsilon^{\rm obs}_{+,N_{\rm pix}}, \epsilon^{\rm obs}_{\times,N_{\rm pix}}\}$, from the $2N_{\rm pix}$ measured ellipticities $\epsilon^{\rm obs}_{+,ij}$ and $\epsilon^{\rm obs}_{+,ij}$, and each observed value is due to signal and noise, $D^{\rm obs}_\alpha = D^{\rm s}_\alpha + D^{\rm n}_\alpha$. Suppose further that we are testing a Gaussian theory that predicts expectation values $\left\langle D^{\rm s}_\alpha D^{\rm s}_\beta\right\rangle = C^{\rm s}_{\alpha\beta}$ (where the theory correlation matrix is given by the unrotated correlation functions discussed in Section 2.3) with a map which has Gaussian noise with a correlation matrix $\left\langle D^{\rm n}_\alpha D^{\rm n}_\beta\right\rangle = C^{\rm n}_{\alpha\beta}$. The likelihood of this theory given the data is

$$\mathcal{L} \propto \exp\{D^{\rm obs}_\alpha [(C^{\rm s} + C^{\rm n})^{-1}]_{\alpha\beta} D^{\rm obs}_\beta\}. \tag{29}$$

For example, if the noise is due entirely to intrinsic source ellipticities, then the noise in each pixel is uncorrelated and the noise between + and × ellipticities is also uncorrelated, so the noise correlation matrix becomes diagonal with entries equal to the variance in each ellipticity, $C^{\rm n}_{\alpha_\beta} = \sigma^2_\epsilon \delta_{\alpha\beta}$. In general, however, the noise correlation matrix will be nondiagonal (Refregier & Brown 1998), and the theory matrix is also non-diagonal. Therefore, for a 10000 deg^2 survey with 20×20 arcmin^2 pixels, the data vector will have 180 000 entries, and evaluation of the likelihood would require inversion of a $180\,000 \times 180\,000$ matrix!

Progress in evaluating the likelihood with good accuracy can be made by working in the Fourier domain instead. In this case, we write the data as a $2N_{\rm pix}$-dimensional vector with the $N_{\rm pix}$ measured Fourier components $\tilde{\gamma}^{\rm obs}_{\rm g}(\boldsymbol{\kappa})$ and $\tilde{\gamma}^{\rm obs}_{\rm c}(\kappa)$ as components. Statistical isotropy and homogeneity guarantee that these have expectation values $\left\langle \tilde{\gamma}^{\rm s}_{\rm g}(\boldsymbol{\kappa})\tilde{\gamma}^{\rm s}_{\rm g}(\boldsymbol{\kappa}')\right\rangle = P^{\rm s}_{\rm gg}(\kappa)\delta_{\boldsymbol{\kappa}\boldsymbol{\kappa}'}$, $\left\langle \tilde{\gamma}^{\rm s}_{\rm g}(\boldsymbol{\kappa})\tilde{\gamma}^{\rm s}_{\rm c}(\boldsymbol{\kappa}')\right\rangle = 0$, and $\left\langle \tilde{\gamma}^{\rm s}_{\rm c}(\boldsymbol{\kappa})\tilde{\gamma}^{\rm s}_{\rm c}(\boldsymbol{\kappa}')\right\rangle = 0$. In other words, the covariance of the Fourier components is diagonal, and since all the c components are expected to be zero, we only need to deal with a $N_{\rm pix} \times N_{\rm pix}$ (rather than $2N_{\rm pix} \times 2N_{\rm pix}$) covariance matrix. Unfortunately, the covariance of the noise in Fourier space will not always be diagonal, unless the noise correlation functions depend only on the separation between

two points and not their relative orientation. This will not necessarily be the case. For example, the noise in interferometric images is generally spatially correlated and has preferred directions (visible as 'stripes' in the noise). This produces spurious ellipticity correlations which depend on the orientation of the source-separation vector (Refregier & Brown 1998). Therefore, the error obtained by assuming the covariance in Fourier space to be diagonal will underestimate the true error. By carrying out a full likelihood analysis on a small patch of the survey and comparing it with the results of the restricted analysis (i.e., that which assumes the Fourier components are all statistically independent) on that same patch, one can determine the degree to which the restricted analysis underestimates the error.

To proceed, we must make the approximation that the covariance of the noise is diagonal in the Fourier domain. Then the power spectrum $P^{\rm n}_{\rm gg}(\kappa)$ of the noise can be obtained from the noise correlation functions, $C^{\rm n}_1(\theta)$ and $C^{\rm n}_2(\theta)$, which are obtained by averaging over all orientations ϕ. With this approximation, both the noise and theory covariance matrices are diagonal in the Fourier domain, and evaluation of the likelihood reduces to evaluation of the usual χ^2. Therefore, if our model consists of a smoothed power spectrum $\mathcal{A}P^{\rm s}_{\rm gg}(\kappa)$ and we are trying to fit for the amplitude $\mathcal{A}$, then each of the $N_{\rm pix}$ measured Fourier components $\boldsymbol{\kappa}$ provides an independent estimator,

$$\mathcal{A}_{\boldsymbol{\kappa}} = \frac{|\tilde{\gamma}^{\rm obs}_{\rm g}(\boldsymbol{\kappa})|^2 - P^{\rm n}_{\rm gg}(\kappa)}{P^{\rm s}_{\rm gg}(\kappa)}, \tag{30}$$

for $\mathcal{A}$, with a variance

$$\sigma^2_{\mathcal{A}_{\boldsymbol{\kappa}}} = \left\langle (\mathcal{A}_{\boldsymbol{\kappa}} - \mathcal{A}_{\boldsymbol{\kappa}})^2 \right\rangle = \frac{2[\mathcal{A}P^{\rm s}_{\rm gg}(\kappa) + P^{\rm n}_{\rm gg}(\kappa)]^2}{[P^{\rm s}_{\rm gg}(\kappa)]^2}. \tag{31}$$

Therefore, an estimator for $\mathcal{A}$ for the entire survey is

$$\widehat{\mathcal{A}} = \frac{\sum_{\boldsymbol{\kappa}} \mathcal{A}_{\boldsymbol{\kappa}}/\sigma^2_{\mathcal{A}_{\boldsymbol{\kappa}}}}{1/\sigma^2_{\mathcal{A}}}, \tag{32}$$

and the variance to this estimator is $\sigma_{\mathcal{A}}$ given by

$$\frac{1}{\sigma^2_{\mathcal{A}}} = \sum_{\boldsymbol{\kappa}} \frac{1}{\sigma^2_{\mathcal{A}_{\boldsymbol{\kappa}}}}. \tag{33}$$

To determine the smallest value of $\mathcal{A}$ which could be distinguished from the noise, we insert the null hypothesis $\mathcal{A} = 0$ into equation (33). To illustrate, suppose that the noise in each component of the ellipticity was Gaussian with variance σ^2_ϵ and independent of each other component, as assumed above. In this case, $P^{\rm n}_{\rm gg}(\kappa) = \sigma^2_\epsilon$. Therefore,

$$\frac{1}{\sigma^2_{\mathcal{A}}} = \frac{1}{2\sigma^4_\epsilon}\sum_{\boldsymbol{\kappa}}[P^{\rm s}_{\rm gg}(\kappa)]^2 \simeq \frac{N^2_{\rm pix}}{2\sigma^4_\epsilon}\int \frac{{\rm d}^2\boldsymbol{\kappa}}{(2\pi)^2}[P^{\rm s}_{\rm gg}(\boldsymbol{\kappa})]^2, \tag{34}$$

or in other words,

$$\frac{\sigma_{\mathcal{A}}}{\mathcal{A}} = \frac{\sqrt{2}\sigma^2_\epsilon}{N_{\rm pix}}\mathcal{I}^{-1/2}_\sigma = \frac{\sqrt{2}\bar{\epsilon}^2}{\bar{n}A}\mathcal{I}^{-1/2}_\sigma, \tag{35}$$

where

$$\mathcal{I}_\sigma \equiv \mathcal{A}^2\int \frac{{\rm d}^2\boldsymbol{\kappa}}{(2\pi)^2}[P^{\rm s}_{\rm gg}(\boldsymbol{\kappa})]^2, \tag{36}$$

and we have used $\sigma^2_\epsilon = \bar{\epsilon}^2/(\bar{n}\theta^2_p)$ and $\theta^2_p = A/N_{\rm pix}$. Equation (35) shows how the signal-to-noise ratio scales with the mean intrinsic source ellipticity $\bar{\epsilon}$, usable density of sources $\bar{n}$ and the survey area A.

4 PREDICTIONS FOR THE FIRST SURVEY

4.1 Preliminaries

We will restrict our analysis to a flat Universe ($\Omega_0 + \Omega_\Lambda = 1$), but will allow for a non-zero cosmological constant Ω_Λ. The scale factor of the Universe, $a(t)$, satisfies the Friedmann equations,

$$\frac{\dot{a}}{a} = H_0 E(z) \equiv H_0\sqrt{\Omega_0(1+z)^3 + \Omega_\Lambda}, \tag{37}$$

where $H_0 = 100\,h\,{\rm km\,s^{-1}\,Mpc^{-1}}$ is the Hubble constant, Ω_0 is the current non-relativistic-matter density in units of the critical density, Ω_Λ is the current contribution of the cosmological constant to closure density, and the dot denotes derivative with respect to time.

We choose the scale factor such that $a_0H_0 = 2$. If we are located at the origin, $\boldsymbol{w} = 0$, then an object at redshift z is at a comoving distance,

$$w(z) = \frac{1}{2}\int_0^z \frac{{\rm d}z'}{E(z')}, \tag{38}$$

and the comoving distance to the horizon (or the conformal time today) is

$$\eta_0 = \frac{1}{2}\int_0^\infty \frac{{\rm d}z'}{E(z')}. \tag{39}$$

4.2 Weak-lensing power spectrum

Given a power spectrum $P(k,z)$ for the mass distribution, the power spectrum for the gravitational potential is

$$P_\phi(k,z) = k^{-4}\left[\frac{3}{2}(a_0H_0)^2\Omega_0(1+z)\right]^2 P(k,z). \tag{40}$$

In linear theory, the time evolution of the power spectrum is given by

$$P(k,z) = P(k,z=0)[D(z)/D(z=0)]^2, \tag{41}$$

where

$$D(z) = \frac{5\Omega_0\,E(z)}{2}\int_z^\infty \frac{1+z'}{[E(z')]^3}\,{\rm d}z', \tag{42}$$

is the linear-theory growth factor (see, e.g., Peebles 1993).

The weak-lensing power spectrum is (Kaiser 1992)

$$P_{\rm gg}(\kappa) = 4\int {\rm d}z\,\frac{{\rm d}w}{{\rm d}z}\left[\frac{g(z)}{w(z)}\right]^2\left[\frac{\kappa}{w(z)}\right]^4 P_\phi(\kappa/w, z), \tag{43}$$

where $g(z)$ is given in terms of the survey redshift distribution, ${\rm d}N/{\rm d}z$, by

$$\frac{g(z)}{w(z)} = \int_z^\infty {\rm d}z'\,\frac{1}{N}\frac{{\rm d}N}{{\rm d}z'}\left[1 - \frac{w(z)}{w(z')}\right]. \tag{44}$$

Inserting equations (40)–(42) into equation (43), we find

$$P_{\rm gg}(\kappa) = \frac{1}{\kappa}\int_{\kappa/\eta_0}^\infty I_\kappa(k)\,P(k,z=0)\,{\rm d}k, \tag{45}$$

where

$$I_\kappa(k) = 144\Omega^2_0[g(w=\kappa/k)]^2[1+z(w=\kappa/k)]^2 \times [D(w=\kappa/k)/D_0]^2. \tag{46}$$

The mean-square variance in a cell with window function $\widetilde{W}(\kappa)$ is

$$\left\langle(\gamma^{\rm s}_{\rm g})^2\right\rangle = \int {\rm d}k\,P(k,0)\,G(k), \tag{47}$$

where

$$G(k) = \int_0^{k\eta_0}\frac{{\rm d}\kappa}{2\pi}|\widetilde{W}(\kappa)|^2\,I_\kappa(k). \tag{48}$$

4.3 Model for the spatial density power spectrum

For the power spectrum, we use

$$P(k) = \frac{2\pi^2}{8}\delta_H^2 (k/2)^n T^2(k_p\,\mathrm{Mpc}/h\Gamma), \tag{49}$$

where $T(q)$ is the usual CDM transfer function, $k_p = kH_0/2$ is the physical wavenumber, and $\Gamma \simeq \Omega_0 h$ is given more accurately in terms of $\Omega_0 h$ and the baryon fraction Ω_b by equations (D-28) and (E-12) in Hu & Sugiyama (1996). For the transfer function, we use (Bardeen et al. 1986),

$$T(q) = \frac{\ln(1+2.34q)/(2.34q)}{[1+3.89q+(16.1q)^2+(5.46q)^3+(6.71q)^4]^{1/4}}. \tag{50}$$

If the power spectrum is normalized to *COBE*, the amplitude δ_H is (Bunn & White 1997)

$$\delta_H(n,\Omega_0) = 1.94\times 10^{-5}\,\Omega_0^{-0.785-0.05\,\ln\Omega_0} \times \exp[a(n-1)+b(n-1)^2]. \tag{51}$$

If primordial density perturbations are a result of inflation, then there will also be a stochastic gravity-wave background which contributes to the *COBE* anisotropy with an amplitude dependent on the spectral index n. In this case, $a = 1$ and $b = 1.97$. If we make no such assumption and suppose that the stochastic gravity-wave background is negligible, then $a = -0.95$ and $b = -0.169$. If we are uncertain of the gravity-wave contribution to *COBE*, then the *COBE* normalization above (with no gravity-wave background) will provide an upper limit to the true amplitude of the power spectrum.

Alternatively, the power spectrum may be normalized at small distance scales through the cluster abundance which fixes σ_8, the variance in the mass enclosed in spheres of radius $8\,h^{-1}$ Mpc, to $\sigma_8 \simeq (0.6\pm 0.1)\Omega_0^{-0.53}$ (Viana & Liddle 1996). In terms of the power spectrum,

$$\sigma_8^2 = \frac{1}{2\pi^2}\int k^2\,\mathrm{d}k\,P(k)\left[\frac{3j_1(k_pR)}{k_pR}\right]^2, \tag{52}$$

where $R = 8\,h^{-1}$ Mpc, and $j_1(x)$ is a spherical Bessel function. Since we are using $a_0 \neq 1$, k_p (rather than k) enters into the argument of the spherical Bessel function.

4.4 Results for the FIRST survey

Fig. 1 shows the weight function $g^2(z)$ that enters into the calculation of the weak-lensing signal for the four FIRST redshift distributions considered by Cress & Kamionkowski (1998) and shown in Fig. 1 therein. Our best estimate for the FIRST redshift distribution is 'DP7 (med-z)' derived from a radio-source luminosity function owing to Dunlop & Peacock (1990), but we also include two other plausible estimates from these authors, 'DP7 (high-z)' and 'DP1,' as well as a redshift distribution derived from a luminosity function due to Condon (1984). For comparison, we also show the weight functions obtained from assuming all sources to be at a redshift of $z_s = 1$ or 2. Below, we calculate the predicted signals with all four FIRST redshift distributions to assess the uncertainty in the predictions from imprecise knowledge of the redshift distribution.

Fig. 2 shows the spatial power spectra of the mass distribution for the four models listed in Table 1. The light dashed curves are the (unnormalized) window functions $G(k)$ needed to calculate the mean-square ellipticity for 1×1 deg^2 pixels and 6×6 arcmin^2 pixels (obtained with our best estimate, DP7 (med-z), for the FIRST redshift distribution). The light dotted curve is the window function needed to calculate σ_8. These window functions illustrate that weak lensing probes power over a wide range of distance scales, and that the ellipticity in 1×1 deg^2 pixels probes the power spectrum on larger scales than σ_8. Here we used the DP7 (med-z) redshift distribution. The weak-lensing window functions would be shifted very slightly to larger scales if we had used the high-z DP7 redshift distribution and to slightly smaller scales if we had used the DP1 or Condon redshift distributions. Figs 3 and 4 show the (unsmoothed)

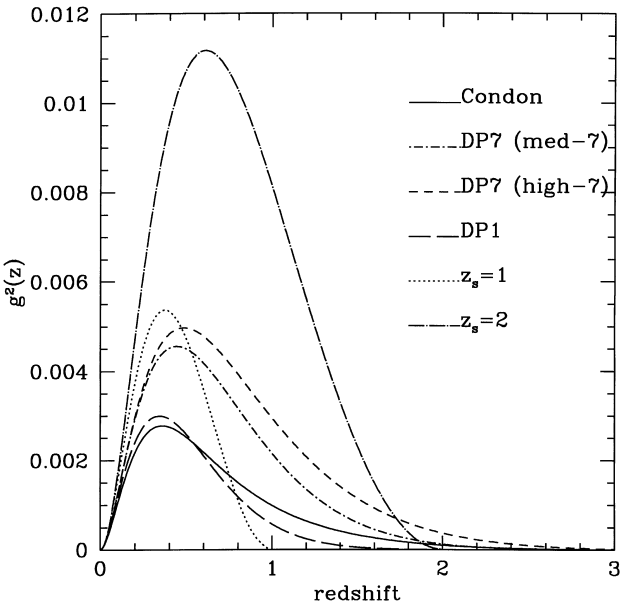

Figure 1. Redshift weight functions $g^2(z)$ for the four FIRST redshift distributions considered in Cress & Kamionkowski (1998). Also shown are $g^2(z)$ that would be obtained if all the sources were at redshift $z_s = 1$ or $z_s = 2$.

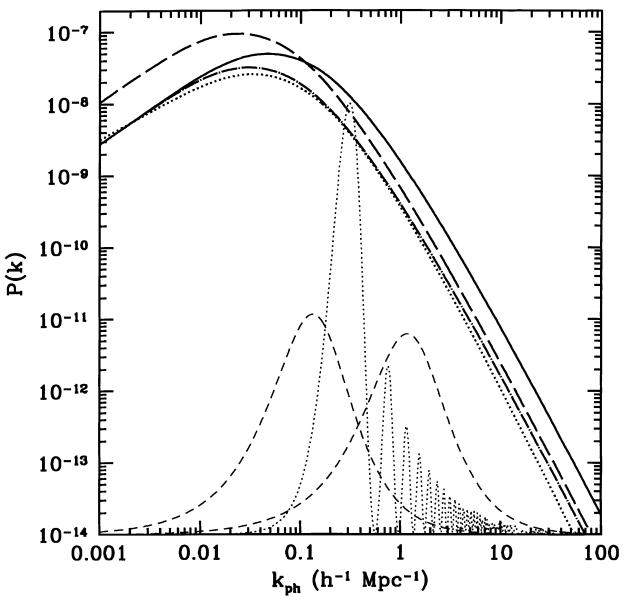

Figure 2. Three-dimensional *COBE*-normalized power spectra $P(k)$ for the four models listed in Table 1. Models 1–4 are represented by solid, dotted, dash, and dot–dash curves, respectively. Also shown (the light dashed curves) are the window functions $G(k)$ needed for calculation of the mean-square ellipticity at $\theta_p = 1^\circ$ and $\theta_p = 6$ arcmin, and the window function (light dotted curve) needed for the calculation of σ_8.

Table 1. Predicted RMS ellipticities, $\langle(\gamma_g^s)^2\rangle^{1/2}$ of FIRST radio sources from weak lensing for $\theta_p = 6$ arcmin, 20 arcmin, and 1° for both *COBE*-normalized and cluster-abundance–normalized power spectra. We also list the values of σ_8 for *COBE*-normalized models.

						$(100\langle(\gamma_g^s)^2\rangle^{1/2})$ *COBE*-normalized			cluster normalized		
Ω	h	n	$\Omega_b h^2$	σ_8	$\sigma_8\Omega_0^{0.53}$	6′	20′	1°	6′	20′	1°
1	0.5	1	0.0125	1.21	1.21	5.2	3.7	2.2	2.6	1.8	1.1
1	0.5	0.8	0.025	0.71	0.71	2.8	2.1	1.4	2.4	1.8	1.2
0.4	0.65	1	0.015	1.07	0.65	2.6	1.9	1.3	2.4	1.8	1.2
1	0.35	1	0.015	0.74	0.74	2.9	2.2	1.5	2.4	1.8	1.2

weak-lensing power spectra and correlation functions for the four (*COBE*-normalized) models listed in Table 1 (again, using the med-z DP7 redshift distribution).

Table 1 lists the predicted rms gradient component of the ellipticity for several flat *COBE*-normalized and cluster-abundance–normalized cold-dark-matter models with and without a cosmological constant for 6×6 arcmin^2 pixels, 30×30 arcmin^2 pixels, and 1×1 deg^2 pixels calculated with equation (47). We used the med-z DP7 redshift distribution for these calculations. For the window function, we use

$$\widetilde{W}(\kappa) = 2J_1(x)/x \qquad \text{with} \qquad x \equiv \kappa\theta_p/\sqrt{\pi}, \tag{53}$$

and θ_p is the pixel size.[1] In all cases, the rms ellipticity scales with the pixel size roughly as $\langle(\gamma_g^s)^2\rangle^{1/2} \propto \theta_p^{-\beta}$ with $\beta = 0.3 - 0.4$. We also list $\sigma_8\Omega_0^{0.53}$ where σ_8 is that obtained when the power spectrum is normalized to *COBE*. Note that if the power spectrum is normalized to $\sigma_8\Omega_0^{0.53} = 0.6$, as indicated by the cluster abundance, then the rms ellipticities are 0.018 and 0.012 for $\theta_p = 20$ arcmin and 1°, independent of the model (except for the $\Omega_0 = 1$, $h = 0.5$ model which differs negligibly). Weak lensing is a result of perturbations in the gravitational potential (rather than the mass distribution), and the amplitude of gravitational-potential perturbations is fixed by the cluster abundance. This is why the weak-lensing power spectrum and correlations functions shown in Figs 3 and 4 for the *COBE*-normalized Model 1 are so much higher than the others: this model predicts a value of $\sigma_8\Omega_0^{0.53}$ significantly larger than the others.

We have checked that our calculations agree reasonably well with those of Jain & Seljak (1997) for the models and redshift distributions they consider. Their work illustrates that non-linear effects (which we have not taken into account) are important only for $\theta_p \lesssim 10$ arcmin. Corrections to the predicted signal owing to non-linear evolution of the power spectrum should increase the weak-lensing signal for $\theta_p \gtrsim 10$ arcmin, but only by a relatively small amount.

Table 2 lists the predictions for the *COBE*-normalized $\Omega_0 = 1$, $h = 0.5$, and $n = 1$ model for the four FIRST redshift distributions. If the high-z DP7 redshift distribution is adopted, rather than the med-z DP7 distribution, then the predicted weak-lensing signal is increased by about 6 per cent. But if the true redshift distribution were more accurately represented by the DP1 or Condon distribution, the signal would be smaller by about 20–25 per cent. Note that the fractional uncertainty in the weak-lensing signal is smaller for larger pixel sizes than it is for smaller pixel sizes.

[1] Actually, this is the window function for circular pixels of the same area. The results should be similar if we use the window function for square pixels.

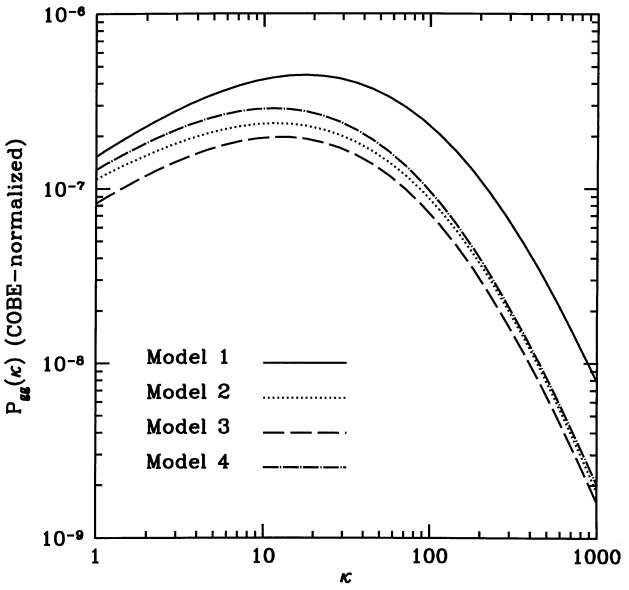

Figure 3. Weak-lensing power spectra $P_{gg}(\kappa)$ for the four (*COBE*-normalized) models listed in Table 1.

4.5 Detectability of a signal with FIRST

Table 1 shows, for example, that for a *COBE*-normalized CDM power spectrum with $\Omega_0 = 1$ and $h = 0.5$, the predicted mean-square ellipticity in 1 deg^2 square pixels is $(0.022)^2$ and $(0.037)^2$ in 20 arcmin^2 pixels. The rms noise in 1° for the survey parameters used above ($A = 10000$ deg^2, $\bar{n} = 40$ deg^{-2}, and $\bar{\epsilon} = 0.4$) is $(0.0075)^2$ and it is $(0.015)^2$ for 20 arcmin^2 pixels, which gives signal-to-noise ratios of 9 and 6 for 1° and 20 arcmin pixels, respectively. If the power spectrum is normalized to the cluster abundance, then the signal is just near the detection threshold. Since the signal increases with smaller pixel size as $\theta_p^{-2\beta}$ (with $\beta = 0.2 - 0.3$) and the noise increases as θ_p^{-1}, the sensitivity decreases slightly with if a smaller smoothing scale is chosen.

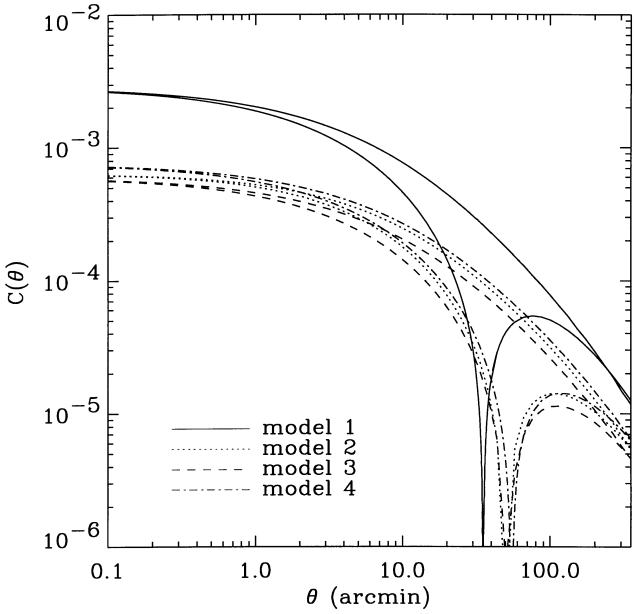

Figure 4. Weak-lensing correlation functions $C_1(\theta)$ and $C_2(\theta)$ for the four (*COBE*-normalized) models listed in Table 1.

Table 2. Predicted RMS ellipticities (in per cent) of radio sources from weak lensing for the *COBE*-normalized Model 1 for 6×6 arcmin^2 and 1×1 deg^2 pixels.

Redshift Distribution	$100 \langle (\gamma_g^s)^2 \rangle^{1/2} (\theta_p = 6')$	$100 \langle (\gamma_g^s)^2 \rangle^{1/2} (\theta_p = 1^\circ)$
DP7 (med-z)	5.2	2.2
DP7 (high-z)	5.6	2.3
DP1	4.0	1.8
Condon	4.2	1.9

However, the sensitivity of the signal can be improved significantly if the full information encoded in the power spectrum is exploited with a maximum-likelihood analysis. For example, for the *COBE*-normalized $\Omega_0 = 1$ and $h = 0.5$ model, $\mathcal{I}_\sigma = 1.6 \times 10^{-10}$ for the window function corresponding to 20 arcmin pixels. From equation (35), the signal-to-noise with this maximum-likelihood technique would be $\mathcal{A}/\sigma_{\mathcal{A}} = 22$, which is much larger than that obtained by just comparing the predicted and measured mean-square ellipticity using either 20 arcmin or 1° pixels. Therefore, a proper maximum-likelihood analysis can improve the sensitivity by a factor of 2–3. Given that the signal for cluster-abundance–normalized power spectra is only on the verge of detectability when only the mean-square ellipticity is measured (i.e., the predicted mean-square ellipticity is only slightly larger than 3σ), we conclude that, with this more sophisticated maximum-likelihood analysis, a high-significance detection ($\gtrsim 6\sigma$) should be possible with these survey parameters.

5 DISCUSSION AND CONCLUSIONS

In this paper we have calculated the predicted ellipticity correlations of FIRST radio sources expected from weak gravitational lensing owing to mass inhomogeneities along the line of sight for several plausible power spectra for the large-scale mass distribution in the Universe. We discussed the tensor Fourier analysis and statistical techniques needed to isolate the signal in the data. The shear field reconstructed from measured ellipticities can be decomposed into a 'gradient' and 'curl' component. Weak lensing predicts the presence of only a gradient component. Measurement of the curl component can be used to look for non-lensing artifacts in the data.

We also estimated the amplitude of a signal which could be detectable with a survey as a function of the source density of the survey, mean intrinsic source ellipticity, and area of the survey. We found that a detection of the signal from cluster-abundance–normalized power spectra could be expected with good statistical significance ($\gtrsim 6\sigma$) with survey parameters which approximate those of FIRST. *COBE*-normalized models produce an even larger signal.

In addition to the statistical errors which we have taken into account, there will be systematic effects in the data which will mimic the effects of weak lensing. However, the most egregious of these effects can be modeled and corrected for (Refregier & Brown 1998; Refregier et al., in preparation) and it should be possible to approach the statistical limits discussed here. Even with a slight degradation of the signal-to-noise expected from systematic effects, the effects of weak lensing should be visible for cluster-abundance–normalized power spectra with a maximum-likelihood analysis. A null result would place strict upper limits on the amplitude of mass (rather than luminous-matter) inhomogeneities in the Universe. Seljak (1997) has recently discussed application of more sophisticated statistical techniques developed primarily for clustering and the cosmic microwave background to weak lensing from large-scale structure. These will be needed for precise determination of the power spectrum for future weak-lensing surveys with better sensitivity.

Although there are several other searches for weak-lensing correlations with optical surveys (e.g., Mould et al. 1994), as well as some recent claimed detections (Villumsen 1995; Schneider et al. 1998), these optical surveys probe the ellipticity correlation function on much smaller angular scales than FIRST, which will probe the correlation function on scales $\gtrsim 1^\circ$. Therefore, by combining the results of these surveys, the weak-lensing power spectrum can be reconstructed over a wide angular range. Although the signal may be more easily detected with optical surveys, these will probe scales where corrections owing to non-linear evolution of the power spectrum may be significant. On the other hand, FIRST will probe the power spectrum in a regime where non-linear effects are small, so the comparison with theory will be less hampered by theoretical uncertainties from non-linear effects.

The Sloan Digital Sky Survey (SDSS) will provide yet another data base with which to look for the effects of weak lensing on large angular scales (Stebbins, McKay & Frieman 1996). However, SDSS sources will typically be at smaller redshifts. Therefore, by comparing results from the SDSS and FIRST, the redshift distribution of the weak-lensing distortions can be disentangled. Since FIRST and the SDSS will cover the same region of the sky, one can also cross-correlate the shear field indicated by FIRST with the foreground density field mapped by the SDSS. This will provide more stringent probes of the power spectrum and should also allow a direct measurement of the bias of SDSS sources.

ACKNOWLEDGMENTS

We thank S. Brown, D. Helfand, N. Kaiser and G. Lewis for useful discussions. This work was supported at Columbia by D.O.E. contract DEFG02-92-ER 40699, NASA NAG5-3091, NSF AST94-19906, and the Alfred P. Sloan Foundation. AB gratefully acknowledges financial support from New York University and University of Victoria, and through an operating grant from NSERC. AR was supported at Princeton by the MAP/MIDEX project.

REFERENCES

Baugh C. M., Efstathiou G., 1993, MNRAS, 265, 145
Bardeen J. M., Bond J. R., Kaiser N., Szalay A. S., 1986, ApJ, 304, 15
Bartelmann M., Schneider P., 1992, A&A, 259, 413
Becker R. H., White R. L., Helfand D. J., 1995, ApJ, 450, 559
Blandford R. D., Saust A. B., Brainerd T. G., Villumsen J. V., 1991, MNRAS, 251, 600
Bunn E. F., White M., 1997, ApJ, 480, 6
Condon J. J., 1984, ApJ, 287, 461
Cress C. M., Kamionkowski M., 1998, MNRAS, 297, 486
Dunlop J. S., Peacock J. A., 1990, MNRAS, 247, 19
Gunn J. E., 1967, ApJ, 150, 737
Hu W., Sugiyama, N., 1996, ApJ, 471, 542
Jain B., Seljak U., 1997, ApJ, in press
Kaiser N., 1992, ApJ, 388, 272
Kaiser N., 1998, ApJ, 448, 26
Kamionkowski M., Kosowsky A., Stebbins A., 1997, Phys. Rev. D, 55, 7368
Knox L., 1995, Phys. Rev. D, 52, 4307
Miralda-Escudé J., 1991, ApJ, 380, 1

Mould J., Blandford R., Villumsen J., Brainerd T., Smail I., Small T., Kellis W. 1994, MNRAS, 271, 31
Peebles P. J. E., 1993, Principles of Physical Cosmology. Princeton Univ. Press, Princeton
Seljak U., 1997, preprint (astro-ph/9711124)
Schneider P., van Waerbeke L., Mellier Y., Jain B., Seitz S., Fort B., 1998, A&A, 333, 767
Stebbins A., McKay T., Frieman J., 1996, in Kochanek C. S., Hewitt J. N., eds, Astrophysical Applications of Gravitational Lensing. IAU, Netherlands, p. 75
Stebbins A., 1996, preprint (astro-ph/9609149)
Viana P. T. P., Liddle A., 1996, MNRAS, 281, 323
Villumsen J. V., 1995, preprint (astro-ph/9507007)
Villumsen J. V., 1996, MNRAS, 281, 369
White R. L., Becker R. H., Helfand D. J., Gregg M.D., 1997, ApJ, 475, 479

This paper has been typeset from a TEX/LATEX file prepared by the author.